Supplementary Materials for

Intercomparison of burned area products and its implication for carbon emissions estimations in the Amazon

Ana Carolina M. Pessôa [1,*], Liana O. Anderson[2], Nathália S. Carvalho[1], Wesley A. Campanharo[1], Celso H. L. Silva Junior[1], Thais M. Rosan[3], João B. C. Reis[2], Francisca R. S. Pereira[1], Mauro Assis[4], Aline D. Jacon[5], Jean P. Ometto[5], Yosio E. Shimabukuro[1], Camila V. J. Silva[6], Aline Pontes-Lopes[1], Thiago F. Morello[7] Luiz E. O. C. Aragão[1,3]

* Correspondence: acmoreirapessoa@gmail.com; Tel.: +55-12-3208-6465

This PDF file includes

Supplementary Materials:

A reference list is provided on the main manuscript.

Introduction

This document includes additional text for providing more information on the (S§1) Above ground biomass map methodology, (S§2) Committed gross carbon emission model, and (S§3) AGB map comparison. Also, eight additional figures (S1 to S8) are included here. Finally, seven supporting tables (S1 to S7) are provided with additional information.

1

Table S1. Overview of fire occurrence available products.

Name	Developer	Scale	Type of information	Time span	Sensors/ inputs	Methods	Spatial resolution	Format	Temporal composition	Limitation	Data access	Reference
MCD14ML	NASA	Global	Active fire	2000 – present	MODIS	The algorithm uses brightness temperatures and reflectance information to eliminate obvious non-fire pixels, and the remain are considered in a subsequent contextual analysis.	1000 m	Vector - points	Monthly – possible to know the burn date within the month	Severe temporal and spatial biases may arise in any MODIS fire time series analysis employing time intervals shorter than about eight days. Cloud obscuration, a lack of coverage, or a misclassification in the land/sea mask may be responsible by known fires that do not appear in the dataset, but with only the information provided in the fire location files this will be impossible to determine.	Open access	[1]
VNP14IMGTDL_NRT	NASA	Global	Active fire	2012 - present	VIIRS	Multispectral contextual algorithm to identify sub-pixel fire activity and other thermal anomalies. It includes information on confidence level, FRP and day or nighttime fire.	375 m	Vector - points	Sub-daily	Although its improved spatial resolution provides greater response over small fires and improved mapping of large fires perimeters, Frequent data saturation prevents sub-pixel fire characterization.	Open access	[2]
Fire cci v.5.0	ESA	Global	Burned area	2001 - 2016	MODIS (MOD09GQ – surface reflectance + MOD09GA – quality flags + MCD14ML – active fires)	Hybrid approach, combining information on active fires and temporal changes in reflectance. Clearly burned pixels are detected, and then a contextual procedure is run to improve the delineation of the burned patch.	250 m	Raster (3 layers) - detection date 0: not burned 1 to 366: day of first detection -1: not observed in the month -2: not burnable - confidence level (1-100) - land cover (extracted from Land Cover CCI maps)	Monthly – possible to know the Julian day of first detection within the month, and consequently to identify pixels that burn more than once during a calendar year	The date of the burned pixel may correspond from one to several days after the actual burning date, depending on image availability and cloud cover. All validation results showed worse performance than MCD64 products from NASA.	Open access	[3]
Fire cci v.5.1	ESA	Global	Burned area	2001 - 2019	MODIS (MOD09GQ – surface reflectance + MOD09GA – quality flags + MCD14ML – active fires)	Hybrid approach, combining information on active fires and temporal changes in reflectance. Clearly burned pixels are detected, and then a contextual procedure is run to improve the delineation of the burned patch.	250 m	Raster (3 layers) - detection date 0: not burned 1 to 366: day of first detection -1: not observed in the month -2: not burnable - confidence level (1-100) - land cover (extracted from Land Cover CCI maps)	Monthly – possible to know the Julian day of first detection within the month, and consequently to identify pixels that burn more than once during a calendar year	The date of the burned pixel may correspond from one to several days after the actual burning date, depending on image availability and cloud cover. Fire cci v.5.1 was found less sensitive (11% lower estimations) than MCD64A1 c6 in tropical and temperate fires in Southern Hemisphere South America. The validation metrics showed an important underestimation of total burned area, with higher omission and commission errors, what could be attributed to the coarse spatial resolution of the input images, which implies missing small-size fires (< 100 ha).	Open access	[4]
FireCCILT10	ESA	Global	Burned area	1982 – 2017 (exception of 1994)	AVHRR	The algorithm uses LTDR and CCI Land Cover products, reflectance and spectral indices as input to a multiannual monthly model generated within Random Forest. MCD64A1 dataset is used as training samples.	0.25°	Raster (it is not binary; it includes how much of each pixel was burned using MCD64A1 as a comparison)	Monthly	Although it has the biggest time span available, its method modeled variables, and their uncertainty is not clear accounted for to build the final product. The validation performed does not consider the entire time span.	Open access	[5]

(To be continued)

Table S1 – Continuation.

Name	Developer	Scale	Type of information	Time span	Sensors/inputs	Methods	Spatial resolution	Format	Temporal composition	Limitation	Data access	Reference
MCD64A1 c6	NASA	Global	Burned area	2000 - present	MODIS	It uses MODIS surface reflectance data coupled with 1 km MODIS active fire observations. The algorithm uses a burn sensitive vegetation index (VI) to create dynamic thresholds that are applied to produce the composite data.	500 m	Raster (5 layers) - Burn Date - Burn Date Uncertainty - Quality Assurance - First Day - Last Day	Monthly – possible to know the date of burn (ordinal day of the calendar year on which the burn occurred)	Burned areas in cropland should generally be treated as low confidence due to the inherent difficulty in mapping agricultural burning reliably. Unable to adequately map the occurrence of small fires, what can cause underestimation of overall burned area. It does not individualize the burnt scars.	Open access	[6]
GWIS	JRC	Global	Burned area	2003 - 2016	MODIS	It corresponds to the post-processing of the MCD64A1 product. To identify individual fire events on a global scale, the methodology consists of grouping the burnt pixels in individual burnt scars using a region growth approach.	500 m	Vector - polygons	Multi-annually – It is provided a vector dataset with the entire time span, but it is possible to know the initial and final burn day of each burnt scar	Although it has the advantage of individualizing the burned areas, since it uses MCD64A1, it also incorporates all limitations inherent of its methodology.	Data availability upon request	[7]
GFED4	UM	Global	Burned area Monthly emissions Fractional contributions of different fire types	1997 - present	MODIS	Its algorithm combine MODIS burned area maps with active fire data from TRMM VIRS, and the ATSR family of sensors. It derived exclusively from MCD64A1 c5.1 aggregated to 0.25° spatial resolution.	0.25°	Raster – it is provided a mean burn-date uncertainty dataset for the daily product	Monthly Daily (from Aug-2000)	It does not include small fires (<100ha) - product GFED4s includes them. It underestimates the extent of cropland burning. Cloud cover degrades the detection of both active fires and fire scars; thus, burned area in persistently cloudy regions may be systematically underestimated. Since it uses MCD64A1, it also incorporates all limitations inherent of its methodology.	Open access	[8]
GABAM	IRSDE / CAS	Global	Burned area	2015	Landsat 8 OLI	Automated algorithm implemented on GEE. It uses reflectance and spectral indices information as input for a Random Forest model. A final step consists on burned area shaping through a region growing approach.	30 m	Raster (binary)	Annually	Landsat coarse temporal resolution might cause omission errors in tropical zones due to the quick recovery of the vegetation surface. The lowest overall accuracy was found on Broadleaved Evergreen Forests, what can trap the use of such methodology on tropical regions. It is not provided an uncertainty for each pixel.	Open access	[9]
Landsat Burned Area	NASA	National - US	Burned area	1984 - present	Landsat TM Landsat ETM+ Landsat OLI	Algorithm based on the Landsat Burned Area Essential Climate Variable algorithm. It is a supervised approach that uses gradient boosted regression models implemented in Python.	30 m	Raster (binary)	Annually - binary annual burn classification	Occasionally some burned area is incorrectly classified as being water.	Open access	[10]
TREES	TREES - INPE	Regional – Brazilian Amazon	Burned area	2006 - 2016	MODIS	It uses a hybrid classification. An LSM is performed. Then, the shade fraction image is segmented and unsupervised classified. Subsequently, a manual edition is performed in order to improve the accuracy of the final map.	250 m	Vector	Annually – each file contains information from June to October. It is possible to know the burn month, but not the burn day.	It is not operational, and its time series continuity is not secure. Besides, it is regional, so its use is restricted to Brazilian Amazon.	Data availability upon request	[11–13]
DETER B	INPE	Regional – Brazilian Amazon	Burned area	2016 - present	WFI AWiFS	The identification of the forest cover change pattern is done by visual interpretation based on five main elements (color, tonality, texture, shape and context) and uses the LSM technique, together with its multispectral image in color composition to the visual interpretation.	64 m	Vector	Annually – it follows the same year pattern that PRODES project (from July to August). It is possible to know the date of the image used to map the burnt scar.	The distinction between burnt scar and degradation classes is not clear. If considered only burnt scar class, the total burned area is underestimated. There is not a long time series to be analyzed. Besides, it is regional, so its use is restricted to Brazilian Amazon.	Open access	[14]

(To be continued)

Table S1 – Continuation.

Name	Developer	Scale	Type of information	Time span	Sensors/inputs	Methods	Spatial resolution	Format	Temporal composition	Limitation	Data access	Reference
Acre Queimadas	UFAC	Regional – Acre	Burned area	1984 - 2016	Landsat TM Landsat OLI	It uses the CLASlite 3.0 software to perform a SLM model. From the fraction it is generated a burn-scar index (BSI) image. Subsequently, the BSI is sliced defining thresholds by trial and error to identify forest-fire scars. There is no standard or fixed threshold for this identification, which changes from scene to scene according to fire intensity, vegetation contrast, and image noise.	30 m	Vector	Annually – it was considered images from September to December	The algorithm can miss some fires because they were not strong enough to reach the canopy, affecting only the understory of the forest. Fires can be also missed if they occur after the date of the image used for mapping or if they occur in small forest fragments. Besides, on the classification process targets like shading by thin clouds and smoke or vegetation under extreme water stress can be confused with burnt scar. It only considers fires in forested areas. For this, it uses a deforestation mask. Besides, it is regional, so its use is restricted to Acre state.	Data availability upon request	[15]
Global Fire Atlas	NASA	Global	Burned area Ignition point	2003 - 2016	MODIS	It uses MCD64A1 c6 to track the dynamics of individual fires to determine the timing and location of ignitions and fire size, duration, daily expansion, fire line length, speed, and direction of spread. The approach uses two filters to account for uncertainties in the day of burn, in order to map the location and timing of fire ignitions and the extent and duration of individual fires. Subsequently, it is tracked the growth dynamics of each individual fire to estimate the daily expansion, fire line length, speed, and direction of spread.	500 m	Vector – polygon and point	Annually – It is possible to know start and end dates for each burnt scar or ignition point. It is also provided daily gridded raster of fire line, speed, direction of spread and day of burn.	The algorithm assumes that fires progress continuously through time and space. If cloud coverage or smoke is persistent fir continuity can break, increasing the risk of artificially splitting single fires into multiple parts. Burn date uncertainty may also lead to multiple "extinction points", outliers in the estimated day of burn along the edges of a fire. The coarse resolution can cause underestimation of overall burned area. Since it uses MCD64A1, it also incorporates all limitations inherent of its methodology.	Open access	[16]

Study area

Table S2. List of Brazilian states included in the study area, their respective total area and forest area within the study area boundaries.

State		State area (km²)	State area within the study area (km²)	Proportion of the state area within the study area (%)	Forest area within the study area (km²)	Forest proportion within the study area (%)
Rondônia	**RO**	237,765	237,765	100	121,777	51
Acre	**AC**	164,124	164,124	100	142,368	87
Amazonas	**AM**	1,559,147	1,413,520	91	1,288,699	91
Roraima	**RR**	224,301	21,393	10	18,475	86
Pará	**PA**	1,247,955	1,110,326	89	742,538	67
Amapá	**AP**	142,829	15,304	11	12,415	81
Tocantins	**TO**	277,721	23,973	9	2,288	10
Maranhão	**MA**	278,157	114,860	41	25,583	22
Mato Grosso	**MT**	903,198	480,699	53	260,016	54
	Total	**5,035,197**	**3,581,964**	**71**	**2,614,158**	**73**

Materials and Methods

Table S3. Total burned area and its intersection area with PRODES 2016.

	Burned area Non-forest + Forest (km²)	Burned area over PRODES 2016 (km²)	%
TREES	35558.6	658.8	1.85
MCD64A1	34514.1	513.1	1.49
GABAM	28193.3	750.8	2.66
Fire_cci	14924.3	243.2	1.63

S§1. EBA Methodology

The EBA map was developed by Environmental Monitoring via Satellite in The Amazon Biome - MSA/Amazon Fund - Subproject 7 - Estimating Biomass in the Amazon (EBA). The above ground biomass (AGB) was estimated at three different levels based on 836 LiDAR transects randomly distributed across 3.5 million km² of the Amazon forest. The methodology was based on Lidar AGB estimates [17] and validated using field inventory AGB data [18]. The Lidar AGB was extrapolated for Amazon biome by using a nonparametric regression method (Random Forest) to model the AGB by using remote sensing data of MODIS vegetation index, Shuttle Radar Topography Mission data (SRTM), precipitation data from the Tropical Rainfall Measuring Mission, Synthetic Aperture Radar data of the Phased Array type L-band Synthetic Aperture Radar and geographic coordinates. The

coefficient of determination and the root mean squared error obtained with the final model of the third level of AGB estimation were $R^2 = 0.7485$ and RMSE = 54.36 Mg ha^{-1}, respectively.

The estimated AGB uncertainty map was calculated propagating the uncertainties through the different levels of biomass estimation, field plots (first level), lidar transect (second level) and satellite (third level). The first and second levels were calculated according to Longo et al. (2016) [17], considering calibration uncertainty, representativeness uncertainty and prediction uncertainty. The wall to wall map of uncertainty was developed propagating the total lidar AGB uncertainty to the all cell covered by AGB map of Amazon biome. This was calculated using the mean and standard deviation of the AGB by the total uncertainty and AGB value of each cell of the lidar transect. Then, it was generated a hundred AGB wall to wall maps using the normal distribution values for AGB, remote sensing variable and random forest regression model. The final uncertainty map was generated calculating the standard deviation of AGB of each cell.

S§2. Committed gross carbon emission model

We adapted the committed gross carbon emission model provided by Anderson et al (2015) [13], adding new data from Silva et al (2018) [19] and adjusting the relationship between biomass before and after fire through a power function. All values compiled for establishing the equation were derived from measurements of AGB within 1 year after fire occurrence (Table S4). This method only accounts for the short-term (1 year) carbon loss, although it is being reported on literature that long-term biomass losses may happened for as much as 30 years after a fire event [19].

The update function is showed in Figure S1, where we found a highly significant relationship between biomass before (control) and after fire ($R^2 = 0.95$).

Table S4. Summary of the data used for developing Equation 1.

Reference	**Location**	**Vegetation type**	**Control (Mg.ha^{-1})**	**Mean AGB after fire (Mg.ha^{-1})**
Kauffman et al. (1994) [20]	Brasília (15º 51'S, 47º63'W)	Cerrado	7.128	2
			7.321	0.237
			8.625	2.226
			10.031	1.604
Cochrane and Schulze (1999) [21]	Tailândia (Central-eastern Pará)	Tropical moist evergreen forest	295	270
Haugaasen et al. (2003) [22]	Rio Maró, westernmost Pará (02°44'S; 55°41'W)	Riverbanks forests	424.3	341.7
Barlow et al. (2002) [23]	Rio Maró, westernmost Pará (02°44'S; 55°41'W)	Terra firme forests	95.4	46.8
			91	54
Alencar et al. (2006) [24]	Paragominas (NE of Pará)	Dense forest with vines	485	339.5
	Santana do Araguaia (South of Pará)	Transitional forest	390	273
	Alta Floresta (North of Mato Grosso)	Open forest	370	259
Alencar et al. (2005) [25]	Alta Floresta (North of Mato Grosso)	Open forest	199	88
Barbosa and Fearnside (1999) [26]	Roraima	Dense forest	237	202.3
Silva et al. (2018) [19]	Acre (southwest region)	Open forest	203	212
	Amazonas (central region)	Dense forest	230	286

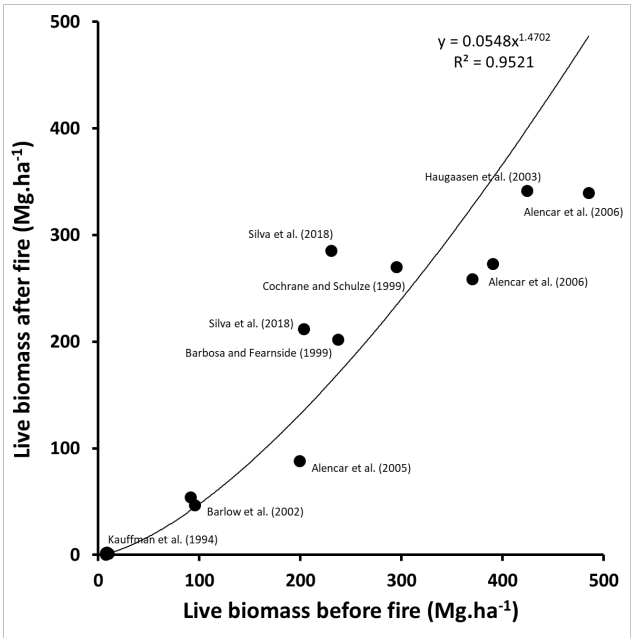

Figure S1. Relationship between initial biomass and remaining biomass after fire events. Plot compiled from literature have burned only once with measurements taken within 1 year of the fire event.

Results

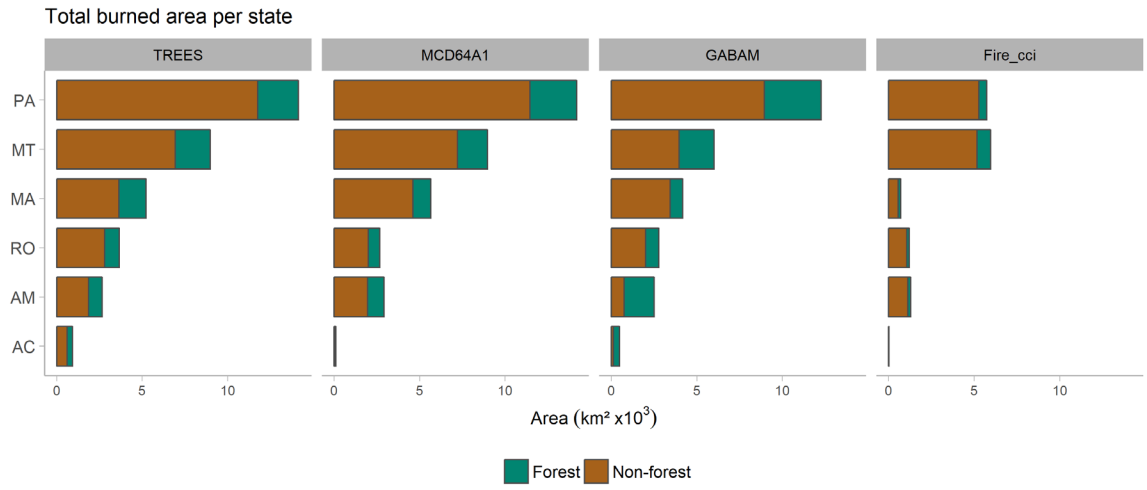

Figure S2. Total burned area mapped by TREES, MCD64A1, GABAM and Fire_cci over forested areas and non-forested areas, per Brazilian state within the study area.S§3. AGB map comparison

For comparation to works that uses Baccini as AGB input to estimate carbon emission, we compare our results using EBA with results using Baccini. Although its relative course resolution compared to Baccini data (30 m), the EBA biomass data includes an uncertainty map, essential for our analysis.

Baccini map is a global dataset that provides AGB for the year 2000 at approximately 30 m spatial resolution. It was used as a reference widely considered in literature [13,17,27,28]. The biomass density (in $Mg.ha^{-1}$) was generated by the statistical relationship between data collected in situ and LiDAR Geoscience Laser Altimeter System (GLAS) data, acquired over 40,000 points. In addition to the field data and GLAS, reflectance data derived from Landsat 7 ETM+, elevation data and biophysical variables are used in the estimation of carbon stock. Random Forest modeling was used to build the statistical relationship [29]. Since the map is from 2000, all deforestations detected by

PRODES between 2001 and 2016 were incorporated into the map. Assuming the characteristics of changes in land use and land cover in the Amazon biome [30], AGB was adjusted considering the pattern observed for pasture areas. Therefore, according to values proposed by [31] for the Amazon, AGB in deforested areas was adjusted to 16.6 Mg ha^{-1}.

For the comparison, both AGB, and AGB uncertainty map were resampled to match Baccini spatial resolution, using the 'nearest' approach. Then, all the methodological steps adopted to estimate carbon emission were repeated using Baccini dataset and the results are presented on Table S5.

Table S5. Difference between the committed gross carbon emission estimates calculated by EBA and Baccini AGB maps.

	Non-forest			*Forest*		
	CGCE EBA (Tg)	**CGCE Baccini (Tg)**	**Difference (EBA - Baccini)**	**CGCE EBA (Tg)**	**CGCE Baccini (Tg)**	**Difference (EBA - Baccini)**
TREES						
AC	0.8988	0.7479	0.1508	0.9008	0.9426	-0.0417
AM	2.8020	2.0821	0.7200	2.2939	2.2647	0.0292
MA	2.2761	6.1801	-3.9040	2.0455	4.8657	-2.8202
MT	6.3525	7.2748	-0.9223	4.1955	5.9858	-1.7903
PA	11.2849	13.5485	-2.2636	5.4341	6.5947	-1.1607
RO	3.9279	3.1502	0.7777	2.0924	2.4000	-0.3076
Study Area	**27.5422**	**32.9835**	**-5.4413**	**16.9621**	**23.0534**	**-6.0913**
MCD64A1						
AC	0.0887	0.0752	0.0135	0.0794	0.0858	-0.0064
AM	2.8355	2.3406	0.4949	2.4044	2.7733	-0.3688
MA	3.1612	7.9061	-4.7450	1.4546	3.0348	-1.5802
MT	6.0644	7.1677	-1.1033	3.3894	4.9422	-1.5528
PA	12.1309	13.9630	-1.8321	6.1418	7.5858	-1.4441
RO	2.7821	2.2084	0.5737	1.6531	1.9518	-0.2987
Study Area	**27.0627**	**33.6611**	**-6.5984**	**15.1227**	**20.3737**	**-5.2510**
GABAM						
AC	0.1441	0.1164	0.0278	0.8514	0.7108	0.1406
AM	1.1535	1.0441	0.1094	3.4177	2.7560	0.6617
MA	2.2655	5.5940	-3.3286	0.8822	1.8524	-0.9702
MT	2.8893	3.8515	-0.9622	3.1854	3.7728	-0.5876
PA	7.7673	10.2850	-2.5178	6.0015	5.6356	0.3660
RO	2.8248	2.1836	0.6413	1.4865	1.4629	0.0236
Study Area	**17.0446**	**23.0747**	**-6.0301**	**15.8246**	**16.1905**	**-0.3659**
Fire_cci						
AC	0.0155	0.0132	0.0023	0.0053	0.0052	0.0001
AM	1.5374	0.9746	0.5627	0.4561	0.4650	-0.0089
MA	0.3023	0.8800	-0.5777	0.1727	0.4412	-0.2686
MT	3.9499	4.8130	-0.8631	1.3196	2.1343	-0.8147
PA	4.6816	4.9836	-0.3019	0.8804	1.1635	-0.2831
RO	1.3372	1.0657	0.2715	0.3085	0.3851	-0.0766
Study Area	**11.8239**	**12.7301**	**-0.9062**	**3.1425**	**4.5944**	**-1.4519**

CGCE = Committed Gross Carbon Emission

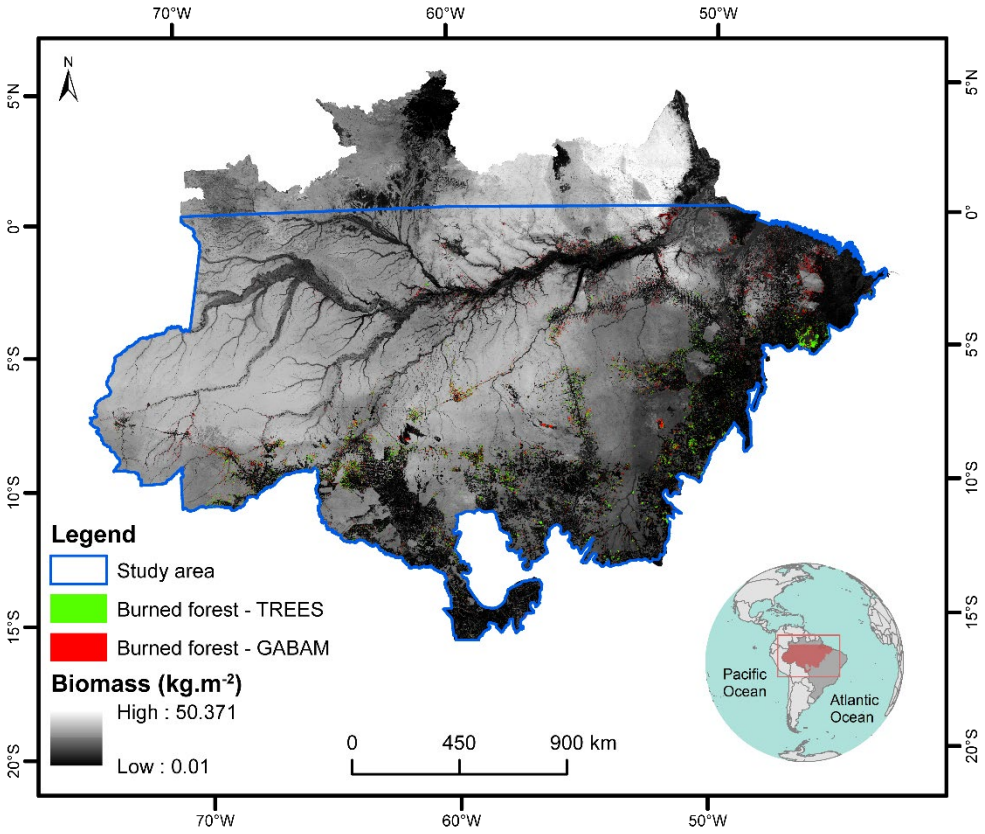

Figure S3. Above ground biomass map from EBA and polygons of burned forest both from TREES and GABAM products.

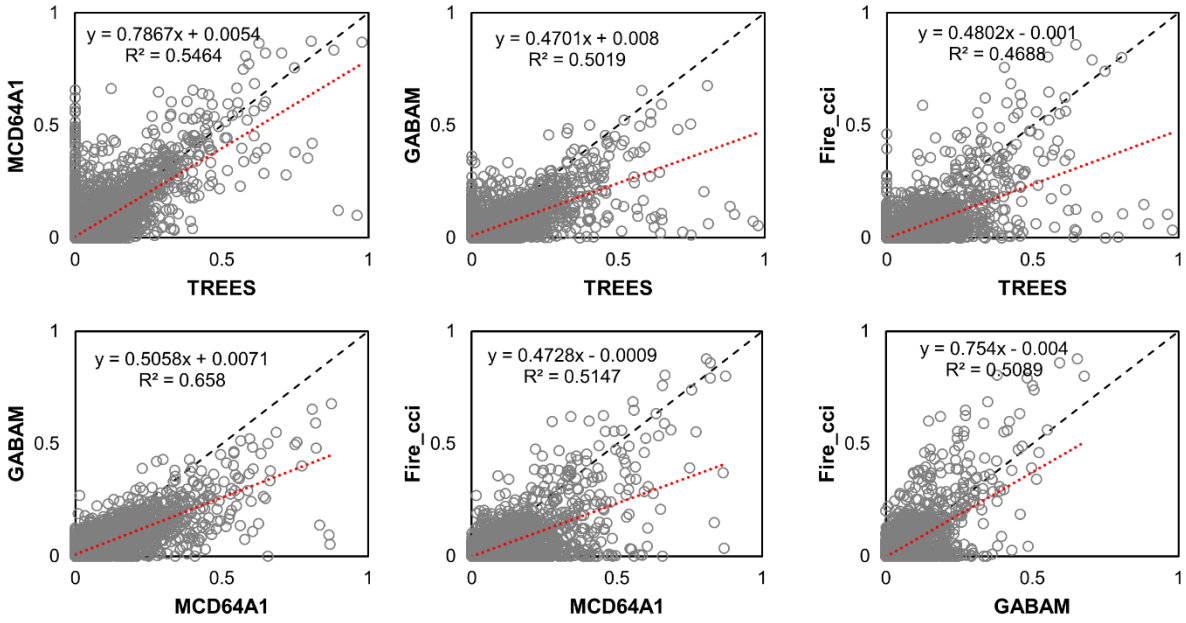

Figure S4. Scatter plots of the percentage of burned area per cell among the different pairs of products. It was considered only cells that presented burned area percentage by at least one product. All relations are statistically significant at 95% confidence level.

Table S6. Mean and stardard deviation of p-values resulted from 10,000 iterations of Kolmogorov-Smirnov two sample test, raffling different samples of 10% of the total grid cells of 10x10km. It was considered only cells that presented burned area percentage by at least one product.

	TREES x MCD64A1	TREES x GABAM	TREES x Fire_cci	MCD64A1 x GABAM	MCD64A1 x Fire_cci	GABAM x Fire_cci
Total (Sample size = 1,434 cells)						
Mean	2.33E-01	0	2.55E-15	0	1.52E-13	0
SD	2.01E-01	0	6.16E-14	0	5.82E-12	0
Forest (Sample size = 1,215 cells)						
Mean	3.12E-01	0	9.56E-18	0	1.14E-13	0
SD	2.74E-01	0	5.35E-16	0	6.74E-12	0
Non-forest (Sample size = 1,229 cells)						
Mean	2.70E-01	5.55E-19	2.31E-14	2.22E-20	3.31E-13	0
SD	2.43E-01	5.44E-17	7.85E-13	1.57E-18	1.44E-11	0

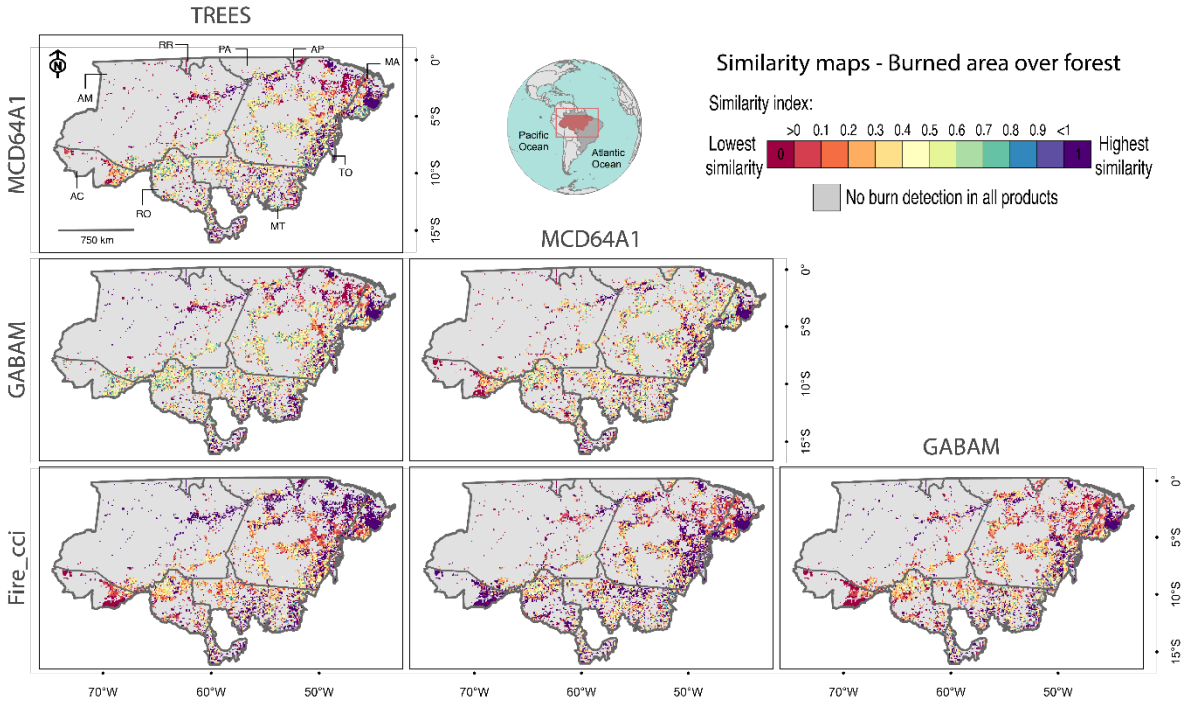

Figure S5. Similarity maps for each burned area product comparison pair, considering burned area over forest. The similarity index was calculated considering only cells over forest that presented burned area detection by at least one product. The similarity index goes from 0 (lowest similarity) highlighted by dark red to 1 (highest similarity) highlighted by dark purple.

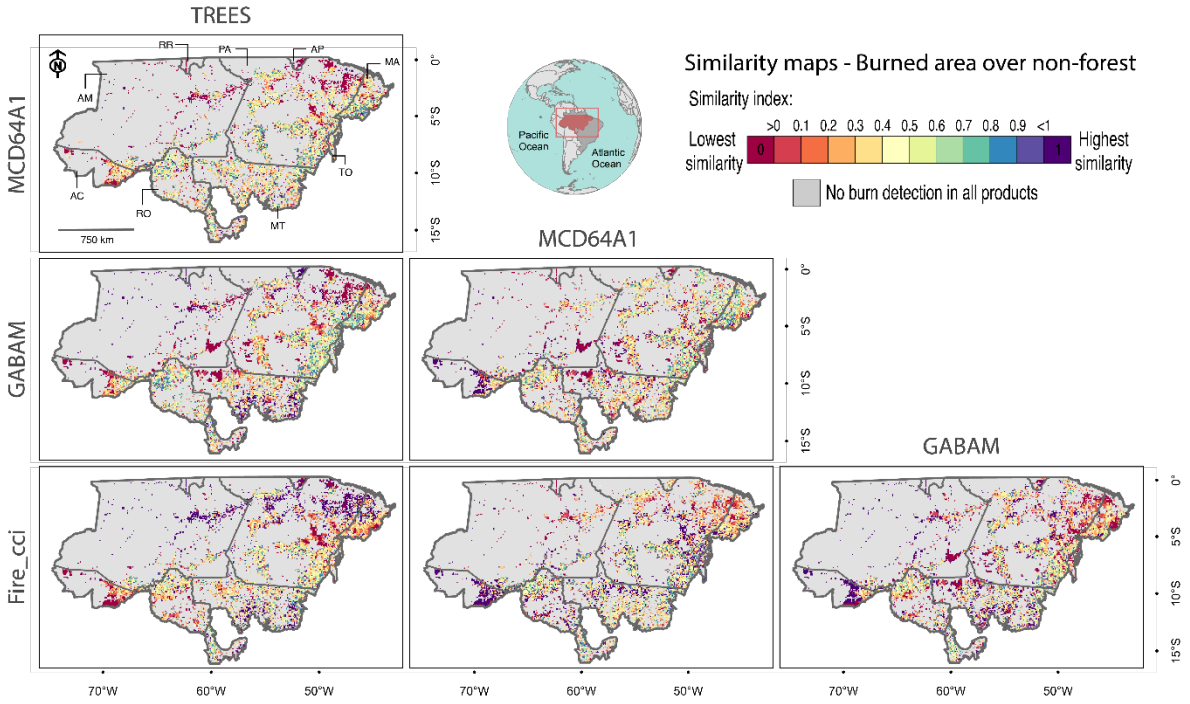

Figure S6. Similarity maps for each burned area product comparison pair, considering burned area over non-forest. The similarity index was calculated considering only cells over non-forest that presented burned area detection by at least one product. The similarity index goes from 0 (lowest similarity) highlighted by dark red to 1 (highest similarity) highlighted by dark purple.

Discussion

Table S7. Total burned area and its intersection area with the hydrography.

Product	State	Burned area [Non-forest + Forest (km²)]	Burned area over hidrography (km²)	%
TREES	AC	925.6	0.3	0.03
	AM	2650.4	11.9	0.45
	MA	5215.3	13.3	0.25
	MT	8981.1	4.6	0.05
	PA	14125.0	11.7	0.08
	RO	3661.1	0.7	0.02
	Study Area	35558.6	42.6	0.12
MCD64A1	AC	113.7	0.0	0.00
	AM	2914.1	299.2	10.27
	MA	5648.5	22.1	0.39
	MT	8967.6	14.9	0.17
	PA	14189.2	160.8	1.13
	RO	2680.9	22.1	0.82
	Study Area	34514.1	519.0	1.50
GABAM	AC	466.8	2.2	0.46
	AM	2507.6	101.3	4.04
	MA	4179.5	16.1	0.38
	MT	6002.5	13.5	0.22
	PA	12270.6	72.0	0.59
	RO	2766.4	38.0	1.38
	Study Area	28193.3	243.0	0.86
Fire_cci	AC	16.9	0.7	4.25
	AM	1294.6	15.5	1.19
	MA	706.1	1.0	0.14
	MT	5959.3	11.1	0.19
	PA	5735.2	4.7	0.08
	RO	1212.2	1.0	0.08
	Study Area	14924.3	34.0	0.23

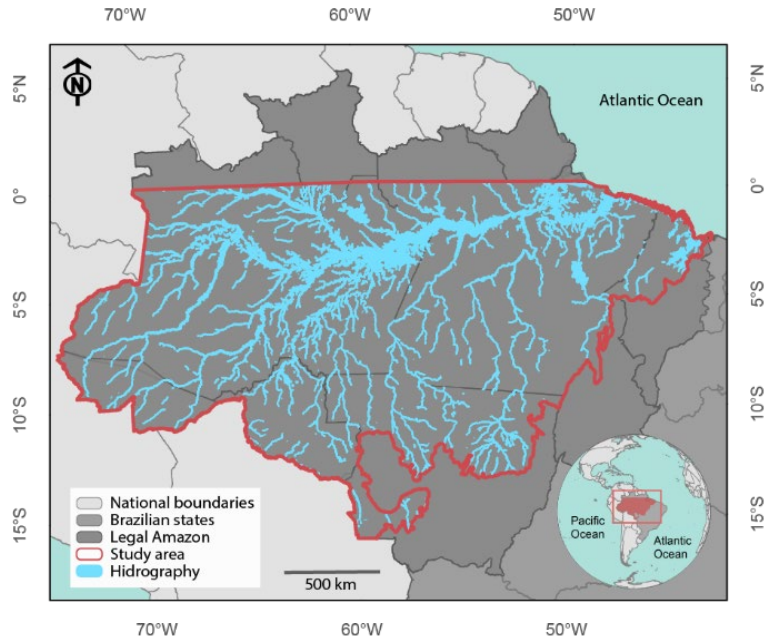

Figure S7. Study area and the hydrography of the region. Source: Hidrography from project PANAMAZÔNIA – INPE (http://www.dsr.inpe.br/laf/panamazonia/).

Graphical abstract

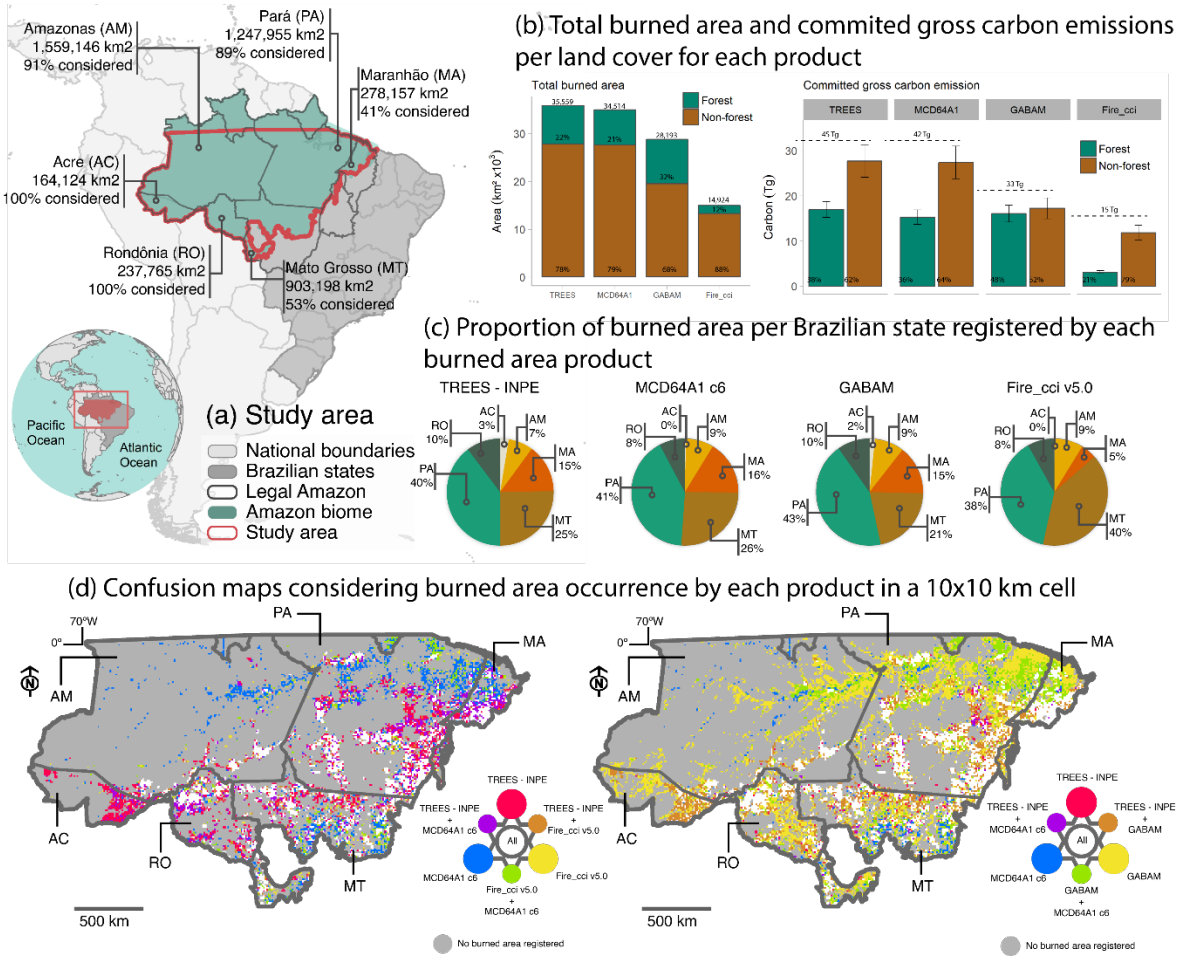

Figure S8. Graphical abstract.

References

1. Bush, M.; Silman, M.; McMichael, C.; Saatchi, S. Fire, climate change and biodiversity in Amazonia: A Late-Holocene perspective. *Philos. Trans. R. Soc. B Biol. Sci.* **2008**, *363*, 1795–1802, doi:10.1098/rstb.2007.0014.
2. Cochrane, M. a Fire science for rainforests. *Nature* **2003**, *421*, 913–919, doi:10.1038/nature01437.
3. Pausas, J.G.; Keeley, J.E. A Burning Story: The Role of Fire in the History of Life. *Bioscience* **2009**, *59*, 593–601, doi:10.1525/bio.2009.59.7.10.
4. Gatti, L.V.; Gloor, M.; Miller, J.B.; Doughty, C.E.; Malhi, Y.; Domingues, L.G.; Basso, L.S.; Martinewski, A.; Correia, C.S.C.; Borges, V.F.; et al. Drought sensitivity of Amazonian carbon balance revealed by atmospheric measurements. *Nature* **2014**, *506*, 76–80, doi:10.1038/nature12957.
5. Aragão, L.E.O.C.; Anderson, L.O.; Fonseca, M.G.; Rosan, T.M.; Vedovato, L.B.; Wagner, F.H.; Silva, C.V.J.; Silva Junior, C.H.L.; Arai, E.; Aguiar, A.P.; et al. 21st Century drought-related fires counteract the decline of Amazon deforestation carbon emissions. *Nat. Commun.* **2018**, *9*, 1–12, doi:10.1038/s41467-017-02771-y.
6. de Azevedo, T.R.; Costa Junior, C.; Brandão Junior, A.; Cremer, M.d.S.; Piatto, M.; Tsai, D.S.; Barreto, P.; Martins, H.; Sales, M.; Galuchi, T.; et al. SEEG initiative estimates of Brazilian greenhouse gas emissions from 1970 to 2015. *Sci. Data* **2018**, *5*, 180045, doi:10.1038/sdata.2018.45.
7. Anderson, L.O.; Aragão, L.E.O.C.; Gloor, M.; Arai, E.; Adami, M.; Saatchi, S.S.; Malhi, Y.; Shimabukuro, Y.E.; Barlow, J.; Berenguer, E.; et al. Disentangling the contribution of multiple land covers to fire-mediated carbon emissions in Amazonia during the 2010 drought. *Glob. Biogeochem. Cycles* **2015**, *29*, 1739–1753, doi:10.1002/2014GB005008.
8. *Brasil Decreto Nº 9.578, de 22 de Novembro de 2018. Consolida atos Normativos Editados pelo Poder Executivo Federal que Dispõem Sobre o Fundo Nacional sobre Mudança do Clima, de que Trata a Lei nº 12.114, de 9 de Dezembro de 2009, e a Política Nacional sobre Mudança do Clima, de que trata a Lei nº 12.187, de 29 de dezembro de 2009*; Diário Oficial da União: Brasília, Brasil, 2018.
9. Aragão, L.E.O..; Malhi, Y.; Barbier, N.; Lima, A.; Shimabukuro, Y.; Anderson, L.; Saatchi, S. Interactions between rainfall, deforestation and fires during recent years in the Brazilian Amazonia. *Philos. Trans. R. Soc. B Biol. Sci.* **2008**, *363*, 1779–1785, doi:10.1098/rstb.2007.0026.
10. Silva Junior, C.; Aragão, L.; Fonseca, M.; Almeida, C.; Vedovato, L.; Anderson, L. Deforestation-Induced Fragmentation Increases Forest Fire Occurrence in Central Brazilian Amazonia. *Forests* **2018**, *9*, 305, doi:10.3390/f9060305.
11. Marengo, J.A.; Tomasella, J.; Alves, L.M.; Soares, W.R.; Rodriguez, D.A. The drought of 2010 in the context of historical droughts in the Amazon region. *Geophys. Res. Lett.* **2011**, *38*, doi:10.1029/2011GL047436.
12. Jiménez-Muñoz, J.C.; Mattar, C.; Barichivich, J.; Santamaría-Artigas, A.; Takahashi, K.; Malhi, Y.; Sobrino, J.A.; Schrier, G. van der Record-breaking warming and extreme drought in the Amazon rainforest during the course of El Niño 2015–2016. *Sci. Rep.* **2016**, *6*, 33130, doi:10.1038/srep33130.
13. Li, W.; Fu, R.; Dickinson, R.E. Rainfall and its seasonality over the Amazon in the 21st century as assessed by the coupled models for the IPCC AR4. *J. Geophys. Res.* **2006**, *111*, D02111, doi:10.1029/2005JD006355.
14. Cox, P.M.; Harris, P.P.; Huntingford, C.; Betts, R.A.; Collins, M.; Jones, C.D.; Jupp, T.E.; Marengo, J.A.; Nobre, C.A. Increasing risk of Amazonian drought due to decreasing aerosol pollution. *Nature* **2008**, *453*, 212–215, doi:10.1038/nature06960.
15. Silva Junior, C.H.L.; Anderson, L.O.; Silva, A.L.; Almeida, C.T.; Dalagnol, R.; Pletsch, M.A.J.S.; Penha, T.V.; Paloschi, R.A.; Aragão, L.E.O.C. Fire Responses to the 2010 and 2015/2016 Amazonian Droughts. *Front. Earth Sci.* **2019**, *7*, 1–16, doi:10.3389/feart.2019.00097.
16. Silva, C.V.J.; Aragão, L.E.O.C.; Barlow, J.; Espirito-Santo, F.; Young, P.J.; Anderson, L.O.; Berenguer, E.; Brasil, I.; Foster Brown, I.; Castro, B.; et al. Drought-induced Amazonian wildfires instigate a decadal-scale disruption of forest carbon dynamics. *Philos. Trans. R. Soc. B Biol. Sci.* **2018**, *373*, 20180043, doi:10.1098/rstb.2018.0043.
17. Giglio, L.; Boschetti, L.; Roy, D.P.; Humber, M.L.; Justice, C.O. The Collection 6 MODIS burned area mapping algorithm and product. *Remote Sens. Environ.* **2018**, *217*, 72–85, doi:10.1016/j.rse.2018.08.005.
18. Pettinari, M.L.; Chuvieco, E. *ESA CCI ECV Fire Disturbance: D3.3.3 Product User Guide—MODIS, Version 1.0*; 2018. Available at: https://www.esa-fire-cci.org/documents (accessed on: 25 October 2020)
19. Shimabukuro, Y.E.; Miettinen, J.; Beuchle, R.; Grecchi, R.C.; Simonetti, D.; Achard, F. Estimating Burned Area in Mato Grosso, Brazil, Using an Object-Based Classification Method on a Systematic Sample of Medium Resolution Satellite Images. *IEEE J. Sel. Top. Appl. Earth Obs. Remote Sens.* **2015**, *8*, 4502–4508, doi:10.1109/JSTARS.2015.2464097.

20. Penha, T.V.; Körting, T.S.; Fonseca, L.M.G.; Silva Júnior, C.H.L.; Pletsch, M.A.J.S.; Anderson, L.O.; Morelli, F. Burned Area Detection in the Brazilian Amazon using Spectral Indices and GEOBIA. *Rev. Bras. Cartogr.* **2020**, *72*, 253–269, doi:10.14393/rbcv72n2-48726.
21. Mouillot, F.; Schultz, M.G.; Yue, C.; Cadule, P.; Tansey, K.; Ciais, P.; Chuvieco, E. Ten years of global burned area products from spaceborne remote sensing—A review: Analysis of user needs and recommendations for future developments. *Int. J. Appl. Earth Obs. Geoinf.* **2014**, *26*, 64–79, doi:10.1016/j.jag.2013.05.014.
22. Humber, M.L.; Boschetti, L.; Giglio, L.; Justice, C.O. Spatial and temporal intercomparison of four global burned area products. *Int. J. Digit. Earth* **2019**, *12*, 460–484, doi:10.1080/17538947.2018.1433727.
23. Padilla, M.; Stehman, S.V.; Ramo, R.; Corti, D.; Hantson, S.; Oliva, P.; Alonso-Canas, I.; Bradley, A.V.; Tansey, K.; Mota, B.; et al. Comparing the accuracies of remote sensing global burned area products using stratified random sampling and estimation. *Remote Sens. Environ.* **2015**, *160*, 114–121, doi:10.1016/j.rse.2015.01.005.
24. Ruiz, J.; Lázaro, J.; Cano, I.; Leal, P. Burned Area Mapping in the North American Boreal Forest Using Terra-MODIS LTDR (2001–2011): A Comparison with the MCD45A1, MCD64A1 and BA GEOLAND-2 Products. *Remote Sens.* **2014**, *6*, 815–840, doi:10.3390/rs6010815.
25. Tsela, P.; Wessels, K.; Botai, J.; Archibald, S.; Swanepoel, D.; Steenkamp, K.; Frost, P. Validation of the Two Standard MODIS Satellite Burned-Area Products and an Empirically-Derived Merged Product in South Africa. *Remote Sens.* **2014**, *6*, 1275–1293, doi:10.3390/rs6021275.
26. Padilla, M.; Stehman, S.; Litago, J.; Chuvieco, E. Assessing the Temporal Stability of the Accuracy of a Time Series of Burned Area Products. *Remote Sens.* **2014**, *6*, 2050–2068, doi:10.3390/rs6032050.
27. Fornacca, D.; Ren, G.; Xiao, W. Performance of Three MODIS Fire Products (MCD45A1, MCD64A1, MCD14ML), and ESA Fire_CCI in a Mountainous Area of Northwest Yunnan, China, Characterized by Frequent Small Fires. *Remote Sens.* **2017**, *9*, 1131, doi:10.3390/rs9111131.
28. Anderson, L.O.; Cheek, D.; Aragao, L.E.; Andere, L.; Duarte, B.; Salazar, N.; Lima, A.; Duarte, V.; Arai, E. Development of a Point-based Method for Map Validation and Confidence Interval Estimation: A Case Study of Burned Areas in Amazonia. *J. Remote Sens. GIS* **2017**, *6*, doi:10.4172/2469-4134.1000193.
29. Pereira, J.M.C.; Mota, B.; Privette, J.L.; Caylor, K.K.; Silva, J.M.N.; Sá, A.C.L.; Ni-Meister, W. A simulation analysis of the detectability of understory burns in miombo woodlands. *Remote Sens. Environ.* **2004**, *93*, 296–310, doi:10.1016/j.rse.2004.01.009.
30. Roy, D.P.; Boschetti, L. Southern Africa validation of the MODIS, L3JRC, and GlobCarbon burned-area products. *IEEE Trans. Geosci. Remote Sens.* **2009**, *47*, 1032–1044, doi:10.1109/TGRS.2008.2009000.
31. Chuvieco, E.; Mouillot, F.; van der Werf, G.R.; San Miguel, J.; Tanase, M.; Koutsias, N.; García, M.; Yebra, M.; Padilla, M.; Gitas, I.; et al. Historical background and current developments for mapping burned area from satellite Earth observation. *Remote Sens. Environ.* **2019**, *225*, 45–64, doi:10.1016/j.rse.2019.02.013.
32. Pereira, J.M.C.; Sá, A.C.L.; Sousa, A.M.O.; Silva, J.M.N.; Santos, T.N.; Carreiras, J.M.B. Spectral characterisation and discrimination of burnt areas. In *Remote Sensing of Large Wildfires*; Springer: Berlin/Heidelberg, Germany, 1999; pp. 123–138.
33. Pleniou, M.; Koutsias, N. Relationships between vegetation indices and different burn and vegetation ratios: A multi-scale approach applied in a fire affected area. In *Proceedings of the SPIE*; Hadjimitsis, D.G., Themistocleous, K., Michaelides, S., Papadavid, G., Eds.; SPIE: Paphos, Cyprus, 2013, Volume 8795, p. 87951I, doi: 0.1117/12.2028349.
34. Boschetti, M.; Stroppiana, D.; Brivio, P.A. Mapping Burned Areas in a Mediterranean Environment Using Soft Integration of Spectral Indices from High-Resolution Satellite Images. *Earth Interact.* **2010**, *14*, 1–20, doi:10.1175/2010EI349.1.
35. Chuvieco, E.; Martín, M.P.; Palacios, A. Assessment of different spectral indices in the red-near-infrared spectral domain for burned land discrimination. *Int. J. Remote Sens.* **2002**, *23*, 5103–5110, doi:10.1080/01431160210153129.
36. Long, T.; Zhang, Z.; He, G.; Jiao, W.; Tang, C.; Wu, B.; Zhang, X.; Wang, G.; Yin, R. 30 m Resolution Global Annual Burned Area Mapping Based on Landsat Images and Google Earth Engine. *Remote Sens.* **2019**, *11*, 489, doi:10.3390/rs11050489.
37. Mithal, V.; Nayak, G.; Khandelwal, A.; Kumar, V.; Nemani, R.; Oza, N. Mapping Burned Areas in Tropical Forests Using a Novel Machine Learning Framework. *Remote Sens.* **2018**, *10*, 69, doi:10.3390/rs10010069.

38. Pleniou, M.; Koutsias, N. Sensitivity of spectral reflectance values to different burn and vegetation ratios: A multi-scale approach applied in a fire affected area. *ISPRS J. Photogramm. Remote Sens.* **2013**, *79*, 199–210, doi:10.1016/j.isprsjprs.2013.02.016.
39. Silva, J.M.N.; Cadima, J.F.C.L.; Pereira, J.M.C.; Grégoire, J.-M. Assessing the feasibility of a global model for multi-temporal burned area mapping using SPOT-VEGETATION data. *Int. J. Remote Sens.* **2004**, *25*, 4889–4913, doi:10.1080/01431160412331291251.
40. Melchiorre, A.; Boschetti, L. Global Analysis of Burned Area Persistence Time with MODIS Data. *Remote Sens.* **2018**, *10*, 750, doi:10.3390/rs10050750.
41. Boschetti, L.; Roy, D.P.; Giglio, L.; Huang, H.; Zubkova, M.; Humber, M.L. Global validation of the collection 6 MODIS burned area product. *Remote Sens. Environ.* **2019**, *235*, 111490, doi:10.1016/j.rse.2019.111490.
42. Bastarrika, A.; Alvarado, M.; Artano, K.; Martinez, M.; Mesanza, A.; Torre, L.; Ramo, R.; Chuvieco, E. BAMS: A Tool for Supervised Burned Area Mapping Using Landsat Data. *Remote Sens.* **2014**, *6*, 12360–12380, doi:10.3390/rs61212360.
43. Anderson, L.O.; Eduardo, L.; De Aragão, C.; De Lima, A. Detecção de cicatrizes de áreas queimadas baseada no modelo linear de mistura espectral e imagens índice de vegetação utilizando dados multitemporais do sensor MODIS/TERRA no estado do Mato Grosso, Amazônia brasileira. *Acta Amaz.* **2005**, *35*, 445–456.
44. Lima, A.; Silva, T.S.F.; de Aragão, L.E.O. e. C.; de Feitas, R.M.; Adami, M.; Formaggio, A.R.; Shimabukuro, Y.E. Land use and land cover changes determine the spatial relationship between fire and deforestation in the Brazilian Amazon. *Appl. Geogr.* **2012**, *34*, 239–246, doi:10.1016/j.apgeog.2011.10.013.
45. Cardozo, F.; Pereira, G.; Shimabukuro, Y.; Moraes, E. Analysis and Assessment of the Spatial and Temporal Distribution of Burned Areas in the Amazon Forest. *Remote Sens.* **2014**, *6*, 8002–8025, doi:10.3390/rs6098002.
46. Shimabukuro, Y.E.; Duarte, V.; Arai, E.; Freitas, R.M.; Lima, A.; Valeriano, D.M.; Brown, I.F.; Maldonado, M.L.R. Fraction images derived from Terra Modis data for mapping burnt areas in Brazilian Amazonia. *Int. J. Remote Sens.* **2009**, *30*, 1537–1546, doi:10.1080/01431160802509058.
47. Shimabukuro, Y.E.; Beuchle, R.; Grecchi, R.C.; Achard, F. Assessment of forest degradation in Brazilian Amazon due to selective logging and fires using time series of fraction images derived from Landsat ETM+ images. *Remote Sens. Lett.* **2014**, *5*, 773–782, doi:10.1080/2150704X.2014.967880.
48. Randerson, J.T.; Chen, Y.; van der Werf, G.R.; Rogers, B.M.; Morton, D.C. Global burned area and biomass burning emissions from small fires. *J. Geophys. Res. Biogeosci.* **2012**, *117*, doi:10.1029/2012JG002128.
49. Artés, T.; Oom, D.; de Rigo, D.; Durrant, T.H.; Maianti, P.; Libertà, G.; San-Miguel-Ayanz, J. A global wildfire dataset for the analysis of fire regimes and fire behaviour. Sci. Data 2019, 6, 296, doi:10.1038/s41597-019-0312-2.
50. Giglio, L.; Randerson, J.T.; van der Werf, G.R. Analysis of daily, monthly, and annual burned area using the fourth-generation global fire emissions database (GFED4). *J. Geophys. Res. Biogeosci.* **2013**, *118*, 317–328, doi:10.1002/jgrg.20042.
51. Andela, N.; Morton, D.C.; Giglio, L.; Paugam, R.; Chen, Y.; Hantson, S.; van der Werf, G.R.; Randerson, J.T. The Global Fire Atlas of individual fire size, duration, speed, and direction. *Earth Syst. Sci. Data Discuss.* **2019**, 1–28, doi:10.5194/essd-2018-89.
52. Shi, Y.; Matsunaga, T.; Yamaguchi, Y. High-Resolution Mapping of Biomass Burning Emissions in Three Tropical Regions. *Environ. Sci. Technol.* **2015**, *49*, 10806–10814, doi:10.1021/acs.est.5b01598.
53. Fanin, T.; van der Werf, G.R. Relationships between burned area, forest cover loss, and land cover change in the Brazilian Amazon based on satellite data. *Biogeosciences* **2015**, *12*, 6033–6043, doi:10.5194/bg-12-6033-2015.
54. Chen, Y.; Morton, D.C.; Andela, N.; van der Werf, G.R.; Giglio, L.; Randerson, J.T. A pan-tropical cascade of fire driven by El Niño/Southern Oscillation. *Nat. Clim. Chang.* **2017**, *7*, 906–911, doi:10.1038/s41558-017-0014-8.
55. Chuvieco, E.; Lizundia-Loiola, J.; Pettinari, M.L.; Ramo, R.; Padilla, M.; Tansey, K.; Mouillot, F.; Laurent, P.; Storm, T.; Heil, A.; et al. Generation and analysis of a new global burned area product based on MODIS 250m reflectance bands and thermal anomalies. *Earth Syst. Sci. Data* **2018**, *10*, 2015–2031, doi:10.5194/essd-10-2015-2018.

56. Lizundia-Loiola, J.; Otón, G.; Ramo, R.; Chuvieco, E. A spatio-temporal active-fire clustering approach for global burned area mapping at 250 m from MODIS data. *Remote Sens. Environ.* **2020**, *236*, 111493, doi:10.1016/j.rse.2019.111493.
57. INPE. *Projeto de Monitoramento do Desmatamento na Amazônia Brasileira por Satélite (PRODES)*; INPE: São José dos Campos, Brazil, 2017.
58. Brando, P.M.; Nepstad, D.C.; Balch, J.K.; Bolker, B.; Christman, M.C.; Coe, M.; Putz, F.E. Fire-induced tree mortality in a neotropical forest: The roles of bark traits, tree size, wood density and fire behavior. *Glob. Chang. Biol.* **2012**, *18*, 630–641, doi:10.1111/j.1365-2486.2011.02533.x.
59. IPCC. *Fifth Assessment Report of the Intergovernmental Panel on Climate Change*; IPCC: New York, NY, USA, 2013.
60. Bivand, R.; Rundel, C. *Rgeos: Interface to Geometry Engine—Open Source ('GEOS') 2018*.
61. R Core Team. *R: A Language and Environment for Statistical Computing 2020*; R Core Team: Vienna, Austria, 2020. Available online at https://www.R-project.org/ (accessed on 30 October 2020).
62. Hijmans, R.J. *Raster: Geographic Data Analysis and Modeling*; 2017.
63. Smirnov, N.V. Estimate of deviation between empirical distribution functions in two independent samples. *Bull. Math. Univ. Moscou* **1939**, *2*, 3–14.
64. Visser, H.; de Nijs, T. The Map Comparison Kit. *Environ. Model. Softw.* **2006**, *21*, 346–358, doi:10.1016/j.envsoft.2004.11.013.
65. RIKS BV. *Map Comparison Kit 3: User Manual*; RIKS BV: Maastricht, The Netherlands, 2013.
66. RIKS BV. *MCK Reader: Methods of the Map Comparison Kit*; RIKS BV: Maastricht, The Netherlands, 2011.
67. Alonso-Canas, I.; Chuvieco, E. Global burned area mapping from ENVISAT-MERIS and MODIS active fire data. *Remote Sens. Environ.* **2015**, *163*, 140–152, doi:10.1016/j.rse.2015.03.011.
68. Giglio, L.; Schroeder, W.; Justice, C.O. The collection 6 MODIS active fire detection algorithm and fire products. *Remote Sens. Environ.* **2016**, *178*, 31–41, doi:10.1016/j.rse.2016.02.054.
69. Justice, C..; Giglio, L.; Korontzi, S.; Owens, J.; Morisette, J..; Roy, D.; Descloitres, J.; Alleaume, S.; Petitcolin, F.; Kaufman, Y. The MODIS fire products. *Remote Sens. Environ.* **2002**, *83*, 244–262, doi:10.1016/S0034-4257(02)00076-7.
70. Meddens, A.J.H.; Kolden, C.A.; Lutz, J.A.; Abatzoglou, J.T.; Hudak, A.T. Spatiotemporal patterns of unburned areas within fire perimeters in the northwestern United States from 1984 to 2014. *Ecosphere* **2018**, *9*, e02029, doi:10.1002/ecs2.2029.
71. Morton, D.C.; DeFries, R.S.; Nagol, J.; Souza, C.M.; Kasischke, E.S.; Hurtt, G.C.; Dubayah, R. Mapping canopy damage from understory fires in Amazon forests using annual time series of Landsat and MODIS data. *Remote Sens. Environ.* **2011**, *115*, 1706–1720, doi:10.1016/j.rse.2011.03.002.
72. Rodrigues, J.A.; Libonati, R.; Pereira, A.A.; Nogueira, J.M.P.; Santos, F.L.M.; Peres, L.F.; Santa Rosa, A.; Schroeder, W.; Pereira, J.M.C.; Giglio, L.; et al. How well do global burned area products represent fire patterns in the Brazilian Savannas biome? An accuracy assessment of the MCD64 collections. *Int. J. Appl. Earth Obs. Geoinf.* **2019**, *78*, 318–331, doi:10.1016/j.jag.2019.02.010.
73. Campanharo, W.; Lopes, A.; Anderson, L.; da Silva, T.; Aragão, L. Translating Fire Impacts in Southwestern Amazonia into Economic Costs. *Remote Sens.* **2019**, *11*, 764, doi:10.3390/rs11070764.
74. da Silva, S.S.; Fearnside, P.M.; de Alencastro Graça, P.M.L.; Brown, I.F.; Alencar, A.; de Melo, A.W.F. Dynamics of forest fires in the southwestern Amazon. *For. Ecol. Manag.* **2018**, *424*, 312–322, doi:10.1016/j.foreco.2018.04.041.
75. Silva, S.S.; Anderson, L.O.; Costa, J.G.; Souza, F.S.C.; Nascimento, E.S.; Silva, I.S.; Pereira, M.P.; Silva, F.V.; Almeida, M.R.N.; Xaud, H.A.M.; et al. *Relatório Executivo: Queimadas 2019—Acre*; UFAC: Cruzeiro do Sul, Acre, Brasil, 2020, 31p., doi: 10.13140/RG.2.2.29291.69927.
76. Barlow, J.; Berenguer, E.; Carmenta, R.; França, F. Clarifying Amazonia's burning crisis. *Glob. Chang. Biol.* **2020**, *26*, 319–321, doi:10.1111/gcb.14872.
77. Giglio, L.; Descloitres, J.; Justice, C.O.; Kaufman, Y.J. An Enhanced Contextual Fire Detection Algorithm for MODIS. *Remote Sens. Environ.* **2003**, *87*, 273–282, doi:10.1016/S0034-4257(03)00184-6.
78. Schroeder, W.; Oliva, P.; Giglio, L.; Csiszar, I.A. The New VIIRS 375m active fire detection data product: Algorithm description and initial assessment. *Remote Sens. Environ.* **2014**, *143*, 85–96, doi:10.1016/j.rse.2013.12.008.
79. Otón, G.; Pettinari, M.L. *ESA CCI ECV Fire Disturbance: D3.3.4 Product User Guide—LTDR, Version 1.0*; 2019. Available at: https://www.esa-fire-cci.org/documents (accessed on 1 November 2020).

80. Hawbaker, T.J.; Vanderhoof, M.K.; Beal, Y.; Takacs, J.D.; Schmidt, G.L.; Falgout, J.T.; Williams, B.; Fairaux, N.M.; Caldwell, M.K.; Picotte, J.J.; et al. Mapping burned areas using dense time-series of Landsat data. *Remote Sens. Environ.* **2017**, *198*, 504–522, doi:10.1016/j.rse.2017.06.027.
81. Diniz, C.G.; Souza, A.A.d.A.; Santos, D.C.; Dias, M.C.; da Luz, N.C.; de Moraes, D.R.V.; Maia, J.S.A.; Gomes, A.R.; Narvaes, I.d.S.; Valeriano, D.M.; et al. DETER-B: The New Amazon Near Real-Time Deforestation Detection System. *IEEE J. Sel. Top. Appl. Earth Obs. Remote Sens.* **2015**, *8*, 3619–3628, doi:10.1109/JSTARS.2015.2437075.
82. Longo, M.; Keller, M.; Dos-Santos, M.N.; Leitold, V.; Pinagé, E.R.; Baccini, A.; Saatchi, S.; Nogueira, E.M.; Batistella, M.; Morton, D.C. Aboveground biomass variability across intact and degraded forests in the Brazilian Amazon. *Glob. Biogeochem. Cycles* **2016**, *30*, 1639–1660, doi:10.1002/2016GB005465.
83. Chave, J.; Réjou-Méchain, M.; Búrquez, A.; Chidumayo, E.; Colgan, M.S.; Delitti, W.B.C.; Duque, A.; Eid, T.; Fearnside, P.M.; Goodman, R.C.; et al. Improved allometric models to estimate the aboveground biomass of tropical trees. *Glob. Chang. Biol.* **2014**, *20*, 3177–3190, doi:10.1111/gcb.12629.
84. Kauffman, J.B.; Cummings, D.L.; Ward, D.E. Relationships of Fire, Biomass and Nutrient Dynamics along a Vegetation Gradient in the Brazilian Cerrado. *J. Ecol.* **1994**, *82*, 519, doi:10.2307/2261261.
85. Cochrane, M.A.; Schulze, M.D. Fire as a Recurrent Event in Tropical Forests of the Eastern Amazon: Effects on Forest Structure, Biomass, and Species Composition1. *Biotropica* **1999**, *31*, 2–16, doi:10.1111/j.1744-7429.1999.tb00112.x.
86. Haugaasen, T.; Barlow, J.; Peres, C.A. Surface wildfires in central Amazonia: Short-term impact on forest structure and carbon loss. *For. Ecol. Manag.* **2003**, *179*, 321–331, doi:10.1016/S0378-1127(02)00548-0.
87. Barlow, J.; Peres, C.A.; Lagan, B.O.; Haugaasen, T. Large tree mortality and the decline of forest biomass following Amazonian wildfires. *Ecol. Lett.* **2002**, *6*, 6–8, doi:10.1046/j.1461-0248.2003.00394.x.
88. Alencar, A.; Nepstad, D.; Diaz, M. del C.V. Forest understory fire in the Brazilian Amazon in ENSO and non-ENSO years : Area burned and comitted carbon missions. *Earth Interact.* **2006**, *10*, 1–17.
89. Alencar, A.A.; Nepstad, D.; Moutinho, P. Carbon emissions associated with forest fires in Brazil. In *Tropical Deforestation and Climate Change*; IPAM: Belém, 2005; p. 132.
90. Barbosa, R.I.; Fearnside, P.M. Incêndios na Amazônia Brasileira: Estimativa da emissão de gases do efeito estufa pela queima de diferentes ecossistemas de Roraima na passagem do evento "El Nino" (1997/98). *Acta Amaz.* **1999**, *29*, 513–534, doi:10.1590/1809-43921999294534.
91. Brinck, K.; Fischer, R.; Groeneveld, J.; Lehmann, S.; Dantas De Paula, M.; Pütz, S.; Sexton, J.O.; Song, D.; Huth, A. High resolution analysis of tropical forest fragmentation and its impact on the global carbon cycle. *Nat. Commun.* **2017**, *8*, 14855, doi:10.1038/ncomms14855.
92. Baccini, A.; Goetz, S.J.; Walker, W.S.; Laporte, N.T.; Sun, M.; Sulla-Menashe, D.; Hackler, J.; Beck, P.S.A.; Dubayah, R.; Friedl, M.A.; et al. Estimated carbon dioxide emissions from tropical deforestation improved by carbon-density maps. *Nat. Clim. Chang.* **2012**, *2*, 182–185, doi:10.1038/nclimate1354.
93. Coutinho, A.C. et al. *Uso e cobertura da terra nas áreas desflorestadas da Amazônia Legal, TerraClass*; Embrapa: Brasília, DF, INPE: Belém, 2013, ISBN 9788570351807.
94. Rosan, T.M. *Estimativa de Emissões de CO_2 por Desmatamento e Degradação Florestal Utilizada como Subsidio para Definição de Municípios Prioritários para Monitoramento e Controle*; Instituto Nacional de Pesquisas Espaciais—INPE: São José dos Campos SP, Brasil: 2017.